33RD CONGRESS
OF THE INTERNATIONAL COUNCIL
OF THE AERONAUTICAL SCIENCES
STOCKHOLM, SWEDEN, 4-9 SEPTEMBER, 2022

ICAS 2022 SWEDEN

RAPID AEROACOUSTIC PLANFORM DESIGN OPTIMIZATION OF INSTALLED PROPELLERS

Tomas Sinnige[1], Wouter de Gruijl[1], Wouter de Haan[1] & Georg Eitelberg[1]

[1]Delft University of Technology, Faculty of Aerospace Engineering, Flight Performance and Propulsion Section, Kluyverweg 1, 2629 HS Delft, the Netherlands.

Abstract

Novel aircraft designs with (distributed) propellers often feature a close coupling between propellers and airframe, leading to unsteady blade loading which impacts propeller efficiency, noise emissions, and vibrations. The goal of this paper is to study the impact of such installation effects on propeller design optimization. A combination of existing, rapid analysis models is used to compute the installed aerodynamic and acoustic propeller performance. These analysis models are coupled to a gradient-based optimization scheme for the design studies. Comparisons are made between optimizations performed with and without taking installation effects into account, analyzing a 5-deg angle-of-attack case and a boundary-layer-ingestion case. The results show that increasing the blade count improves aerodynamic and acoustic performance both for isolated and installed configurations. Furthermore, the acoustic performance is improved significantly by decreasing the blade tip Mach number, albeit with associated efficiency penalty. For the nonuniform inflow fields considered, accounting for installation effects inside the optimization procedure did not lead to large benefits in terms of aerodynamic and acoustic performance compared to the isolated design. For the 5-deg angle-of-attack case, the installed design was similar to the design for symmetric inflow, with negligible change in propeller efficiency and at most 0.5 dB noise reduction. For the boundary-layer-ingestion case, the installed design featured increased solidity and decreased twist, resulting in 0.4% lower energy consumption compared to the design for symmetric inflow. Acoustic performance was not evaluated for this case. Future work will focus on the sensitivity of the results to the blade tip Mach number, the impact of sweep and airfoil design on installed propeller performance, and acoustic optimization of installed configurations with more complex nonuniform inflow fields.

Keywords: Propeller design, propeller performance, propeller noise, propeller-airframe interaction

1. Introduction

Propellers can provide aircraft propulsion with exceptionally high aerodynamic efficiency. The need for more sustainable aviation and an increasing demand for short-range passenger transportation has led to a renewed interest in propellers by the research community. However, as opposed to the high aerodynamic efficiency, the acoustic performance of propellers is not as favorable. Therefore, in order to make propellers more attractive for application on future aircraft, their noise emissions need to be minimized by improving blade design and propeller operating conditions while maintaining high aerodynamic efficiency.

The acoustic emissions from aircraft propellers are dominated by tonal noise due to blade volume and loading (thrust and torque) [1]. For isolated propellers in uniform inflow (i.e. zero degree angle of attack and sideslip), these sources are constant in the circumferential direction. However, when installed on the aircaft, the propeller experiences a nonuniform inflow which results in unsteady blade loading. This unsteady blade loading is responsible for an additional noise source and thus modifies the acoustic emissions. The directivity pattern becomes more complex than for the isolated propeller, featuring lobes in the circumferential direction and increased noise levels especially around the propeller axis [1].

Traditional propeller design studies have focused on isolated propellers in uniform inflow. Multi-objective optimizations for minimum sound-pressure level and maximum aerodynamic efficiency have been performed by Marinus [2] using RANS simulations coupled with a time-domain acoustic solver. Others [3, 4, 5, 6] have taken a similar approach with lower-fidelity aerodynamic analysis tools coupled to comparable acoustic solvers, either in time-domain or frequency domain. These studies have identified planform design and operational variables that are dominant for achieving maximum aeroacoustic performance, such as blade count, rotational frequency, diameter, and radial chord distribution. However, the optimum design for an isolated propeller in uniform inflow does not necessarily provide the best performance for a realistic installed configuration. A notable exception is the work by Pagano et al. [7], which describes an aeroacoustic optimization of a propeller installed in a pusher configuration downstream of a wing. By including the installation effects into the optimization routine, a significant noise reduction was achieved in the installed configuration through planform modifications (mostly sweep) in the outboard segment of the blade. However, this work was done with codes with relatively high computational cost, which makes it less suitable for preliminary design studies.
The goal of the present paper is to present a rapid design method for aeroacoustic optimization of the planform of installed propellers, and apply it to test whether performance enhancements are achieved by accounting for installation effects during the preliminary planform design of propellers. Different cases of nonuniform inflow are considered, and the resulting impact on optimum propeller design and performance is assessed. For simplicity, structural modeling is ignored in this work, but bounds on design variables are imposed such as to achieve realistic blade shapes. The results provide insight into the potential value of planform optimization for prescribed nonuniform inflow conditions, and its impact on the installed aerodynamic and acoustic performance of the propeller.

2. Optimization Framework

Optimizations were performed to assess the tradeoff between aerodynamic and acoustic propeller performance, and the impact of installation effects on resulting optimal designs. Since initial work showed that the aerodynamic and acoustic objectives were conflicting, a two-stage approach was taken. First, a purely aerodynamic optimum was searched: the planform design that led to minimum energy consumption (based on shaft power) for given operational conditions. Subsequently, optimal designs were defined that featured minimum noise emissions for predefined accepted penalties in energy consumption with respect to the aerodynamic optimum. This approach was expected to provide more insight into the tradeoff between aerodynamic and acoustic performance than when using a single objective function with weighted aerodynamic and acoustic performance metrics.

2.1 Test Case

The optimizations were done for a hypothetical test case with operational conditions derived from a small two-seat aircraft. Only the climb and cruise parts of the mission were considered, with corresponding operational conditions and constraints listed in Table 1. For the selected operational conditions, the tip Mach number is limited to about 0.50. Compared to representative turboprop passenger aircraft, this is a relatively low value. However, for the purpose of this paper this was considered acceptable, since the main goal is to test whether accounting for installation effects during the design is beneficial or not. The optimization methodology would be equally applicable to cases with higher tip Mach numbers. For such cases, the aerodynamic analysis model may need to be revised to improve the modeling of compressibility effects.
Using the selected mission definition, three different cases were studied to assess the impact of installation effects on the optimal propeller designs:

1. Uniform inflow: constant velocity in the streamwise direction and zero velocity in lateral and vertical directions. This condition is representative of the isolated propeller in undisturbed inflow and is used as baseline.

2. Nonzero angle of attack: inflow field corresponding to a reference nacelle without propeller at an angle of attack of 5 deg.

Table 1 – Operational conditions and constraints.

Parameter	Climb (cl)	Cruise (cr)
Altitude [m]	100	1000
Freestream velocity [m/s]	38	50
Thrust [N]	830	480
Time [min]	6	30
Max. engine power [kW]	45	30
RPM range [1/min]	1000-2000	
Max. propeller diameter [m]	1.5	

3. Boundary-layer ingestion: fuselage boundary layer with approximate size of the propeller disk resulting in a velocity deficit in the streamwise direction with associated nonzero lateral and vertical velocity components. Vertical-tailplane wake is also included, resulting in an additional nonuniformity in the circumferential direction .

2.2 Objective Functions and Constraints

Different objective functions were used in the optimization studies. A distinction is made between the aerodynamic and acoustic optimization studies.

2.2.1 Aerodynamic Optimization

Baseline optimizations were performed with an objective function focused on aerodynamic performance. In order to describe the performance over the entire mission, the objective for the optimization was based on the sum of the energy consumption E (based on shaft power P) during each of the considered mission segments:

$$E = \sum_{i=1}^{N} E_i = \sum_{i=1}^{N} P_i t_i, \tag{1}$$

with index i referring to the mission segment, N to the number of mission segments considered ($N = 2$ in the present study), and t to the time of each mission segment. Note that only the propeller is considered, hence all quantities are defined at the shaft. Any other losses in the power train (engine, transmission, etc.) are not accounted for. Constant operational conditions and propeller performance were assumed per mission segment, as listed in Table 1.
The objective function f_{aero} of the optimization problem was defined by scaling this energy consumption with the value obtained with the initial design:

$$f_{\text{aero}} = \frac{E}{E_0}. \tag{2}$$

Equality constraints were defined to make sure the propellers delivered the required thrust in both climb and cruise segments (Table 1):

$$\vec{g}_{\text{aero}} = \begin{bmatrix} \frac{T_{\text{cl}}}{T_{\text{cl}_{\text{req}}}} - 1 \\ \frac{T_{\text{cr}}}{T_{\text{cr}_{\text{req}}}} - 1 \end{bmatrix} = 0. \tag{3}$$

Inequality constraints were defined to limit the total shaft power requested from the engine:

$$\vec{h}_{\text{aero}} = \begin{bmatrix} \frac{P_{\text{cl}}}{P_{\text{cl}_{\text{max}}}} - 1 \\ \frac{P_{\text{cr}}}{P_{\text{cr}_{\text{max}}}} - 1 \end{bmatrix} \leq 0. \tag{4}$$

2.2.2 Acoustic Optimization

The acoustic optimizations were performed with an objective function focused on the propeller noise emissions, defined in terms of the thrust-scaled sound pressure level $TSSP$ [9]:

$$TSSP = 20 \log_{10} \left(\frac{p_{\text{rms}} D^2}{T} \right) \tag{5}$$

The $TSSP$ scales the acoustic pressure at the observer location with the pressure jump across the propeller disk (in the actuator-disk approximation) and was used to guarantee a physics-based scaling of the propeller noise [9]. Since the thrust levels were constrained during the optimization and it was decided to fix the diameter to the maximum possible value ($D = 1.5\text{m}$), the $TSSP$ values were at a fixed offset from the conventionally used sound pressure level SPL for the two mission segments considered ($SPL_{\text{cl}} = TSSP_{\text{cl}} + 145.3$ dB, $SPL_{\text{cr}} = TSSP_{\text{cr}} + 140.6$ dB).
The objective function of the acoustic optimization problem was to minimize the thrust-scaled sound pressure level in the climb phase, since this mission segment was considered critical for community noise hindrance. The results were scaled with respect to the initial condition:

$$f_{\text{acoustic}} = \frac{TSSP_{\text{cl}}}{TSSP_{\text{cl}_0}}. \tag{6}$$

The $TSSP$ level was obtained as an average over a surface positioned at vertical offset $h = 100$ m below the propeller. In axial direction, samples were taken at axial directivity angles $\theta = 60, 90, 120$ deg, while in the circumferential direction, samples were taken at circumferential directivity angles $\phi = 150, 160, 170, 180, 190, 200, 210$ deg. Therefore, acoustic pressures were obtained at 21 grid points, which were averaged before converting to the $TSSP$ metric. The variation in circumferential direction was only considered for the installed configurations.
The same constraints were used as for the aerodynamic optimization to match the requirements in terms of thrust per mission segment (Eq. 3) and maximum shaft power (Eq. 4). To also account for the aerodynamic performance in the acoustic optimization, an inequality constraint was added that limited the energy consumption over the mission. This inequality constraint was defined based on a fraction of energy increase ΔE_{tol} defined with respect to the lowest possible energy consumption as obtained from the aerodynamic optimization E^*_{aero}. The complete set of constraints for the acoustic optimization then became:

$$\vec{g}_{\text{acoustic}} = \begin{bmatrix} \frac{T_{\text{cl}}}{T_{\text{cl}_{\text{req}}}} - 1 \\ \frac{T_{\text{cr}}}{T_{\text{cr}_{\text{req}}}} - 1 \end{bmatrix} = 0, \tag{7}$$

$$\vec{h}_{\text{acoustic}} = \begin{bmatrix} \frac{P_{\text{cl}}}{P_{\text{cl}_{\text{max}}}} - 1 \\ \frac{P_{\text{cr}}}{P_{\text{cr}_{\text{max}}}} - 1 \\ \frac{E - E^*_{\text{aero}}}{\Delta E_{\text{tol}}} - 1 \end{bmatrix} \leq 0. \tag{8}$$

2.3 Design Variables & Geometry Parameterization

Design variables were considered related to the propeller operating conditions and geometry. In terms of operating conditions, the collective pitch angle and advance ratio in the two different flight conditions were included:

- Pitch setting at blade tip in climb: $\beta^{\text{tip}}_{\text{cl}}$
- Pitch setting at blade tip in cruise: $\beta^{\text{tip}}_{\text{cr}}$
- Advance ratio in climb: $J_{\text{cl}} = \frac{V_{\text{cl}}}{n_{\text{cl}} D}$
- Advance ratio in cruise: $J_{\text{cr}} = \frac{V_{\text{cr}}}{n_{\text{cr}} D}$

In the optimization procedure, the pitch settings were defined at the blade tip to simplify the definition of the parameterized radial twist distribution (which could now be set to 0 at the tip). In the analysis and presentation of the results, the pitch and twist distributions were shifted to the more conventional definition with the collective pitch setting defined at $r/R = 0.7$ and thus zero blade twist at $r/R = 0.7$.
The propeller geometry was defined by the following parameters:

- Diameter: D
- Number of blades: N_B
- Radial chord distribution: $c(r)$

- Radial twist distribution: $\theta(r)$
- Radial mid-chord-alignment distribution: $MCA(r)$
- Radial face-alignment distribution: $FA(r)$
- Radial airfoil distribution

The radial distributions of planform design parameters were parameterized to limit the number of design variables and guarantee smooth distributions. Bézier curves were used with 4 control points, with the first one fixed at the blade root and the last one at the blade tip, as shown in Fig. 1. Because of the fixed spanwise positions of the first and last control points, the radial distribution of blade chord was defined by 6 variables. For twist only 5 variables were required because the value at the blade tip was fixed to 0.

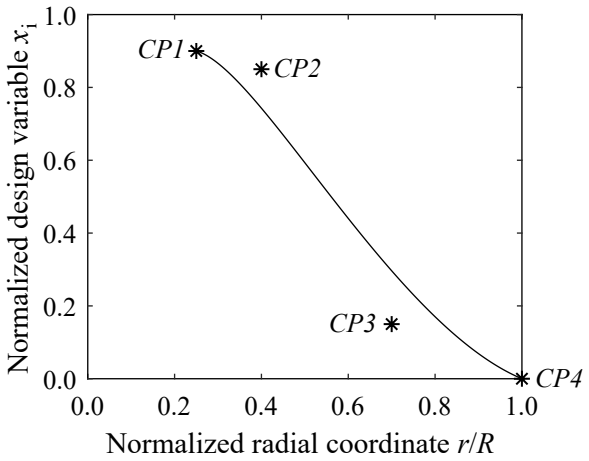

Figure 1 – Example parameterization with Bézier curve with 4 control points.

To limit the number of design variables and complexity of the optimization problem, simplifications were introduced:

- The diameter was fixed to the maximum accepted value of 1.5 m (Table 1) because minimum disk loading is beneficial for aerodynamic efficiency.
- The number of blades was not included inside the optimization. Instead, separate optimizations were performed for each blade count considered: 3, 4, 5, and 6. A blade count of 2 was also used, but it was found that the thrust requirements were too high to obtain a feasible solution for this condition within the bounds on the design variables.
- Blade sweep (mid-chord alignment) and lean (face alignment) were set to zero along the blade span and not modified. Sweep is known to be an effective design variable to reduce noise emissions of isolated propellers [6] and for the installed configuration the potential beneficial impact of sweep can be expected to be even more pronounced. However, the performance predictions for swept propeller blades obtained from the selected aerodynamic analysis model were considered insufficiently accurate at this stage of the work.
- The airfoils were not modified with respect to the baseline design for simplicity. The baseline propeller featured modified ARA-D airfoils with maximum thickness of about 15-20% on the inboard part of the blade, down to 5% near the tip. The camber was about 2-3% on the inboard part of the blade, increasing up to 5% near the sections with highest loading.

The result was an optimization problem with 15 design variables, performed for each individual value of blade count considered. Bounds were defined based on the information provided in Table 1 and considerations regarding structural feasibility of the blade planforms, such as the lower bound on the chord distribution. Table 2 provides an overview.

Table 2 – Bounds on the design variables.

Parameter	Lower	Upper
$\beta_{\mathrm{cl}}^{\mathrm{tip}}$ [deg]	0	60
$\beta_{\mathrm{cr}}^{\mathrm{tip}}$ [deg]	0	60
J_{cl}	0.76	1.52
J_{cr}	1.00	2.00
$(c/R)_{\mathrm{CP1}}^{c(r)}$	0.066	0.200
$(c/R)_{\mathrm{CP2}}^{c(r)}$	0.066	0.200
$(c/R)_{\mathrm{CP3}}^{c(r)}$	0.066	0.200
$(c/R)_{\mathrm{CP4}}^{c(r)}$	0.066	0.200
$(r/R)_{\mathrm{CP2}}^{c(r)}$	0.23	1.00
$(r/R)_{\mathrm{CP3}}^{c(r)}$	0.23	1.00
$\theta_{\mathrm{CP1}}^{\theta(r)}$ [deg]	0	60
$\theta_{\mathrm{CP2}}^{\theta(r)}$ [deg]	0	60
$\theta_{\mathrm{CP3}}^{\theta(r)}$ [deg]	0	60
$(r/R)_{\mathrm{CP2}}^{\theta(r)}$	0.23	1.00
$(r/R)_{\mathrm{CP3}}^{\theta(r)}$	0.23	1.00

2.4 Initial Condition

A random initial point was used for each optimization. Random numbers were generated in the range from 0 to 1. These numbers were then used as the scaled (from lower to upper bound) value of the design variables. For each condition, multiple optimizations were run with different (random) initial points to check for local optima. It was verified that these solutions were similar in terms of both objective function and design variables. The converged solution with the lowest value of the objective function was considered as the final design for each condition.

2.5 Optimization Algorithm and Tolerances

Gradient-based optimization was performed using a sequential quadratic programming method. Tolerances on the objective function convergence, maximum constraint violation, and minimum change in design variables were set to 10^{-4}, 10^{-4}, and 10^{-5}, respectively.

3. Analysis Methods

The aeroacoustic optimization of installed propellers requires analysis models that predict the propeller performance and noise emissions for a given blade planform design and operational conditions. The aerodynamic and acoustic analysis models are discussed separately.

3.1 Propeller Aerodynamics

The propeller blade loads were computed using the method described in Ref. [8]. This method consists of three steps: definition of the nonuniform inflow field, computation of the propeller performance in undisturbed inflow (isolated propeller), and computation of the installed propeller performance.

3.1.1 Inflow Fields

The inflow fields to the propeller are defined in terms of the spatial distributions of the three velocity components in a Cartesian coordinate system at the position of the propeller disk. As mentioned before, three different cases are considered: uniform inflow, 5 deg angle of attack, and boundary-layer-ingestion inflow. The nonuniform inflow fields were obtained from RANS simulations without power effects that were performed as part of earlier work. Since for this paper only the differences between designs for installed and uninstalled configurations are of interest, these inflow fields should only be considered as examples that are used to test the design methodology. Therefore, the specifics of

the numerical simulations that led to these inflow fields are not discussed in the paper. The simulations were performed with slightly different hub geometries than considered in this work. Missing data inside the hub region was replaced by the freestream velocity for the axial component, and zero velocity for the lateral and vertical components. Considering the low blade loading on the inboard parts of the blades, this choice will have had minimal impact on the results.
Figure 2 plots the resulting three inflow fields in terms of the axial, lateral, and vertical velocity components. Note that the inflow fields are assumed to be constant in time. The time-dependent loading of the propeller is thus solely due to the movement of the blades through the steady spatially nonuniform inflow field.

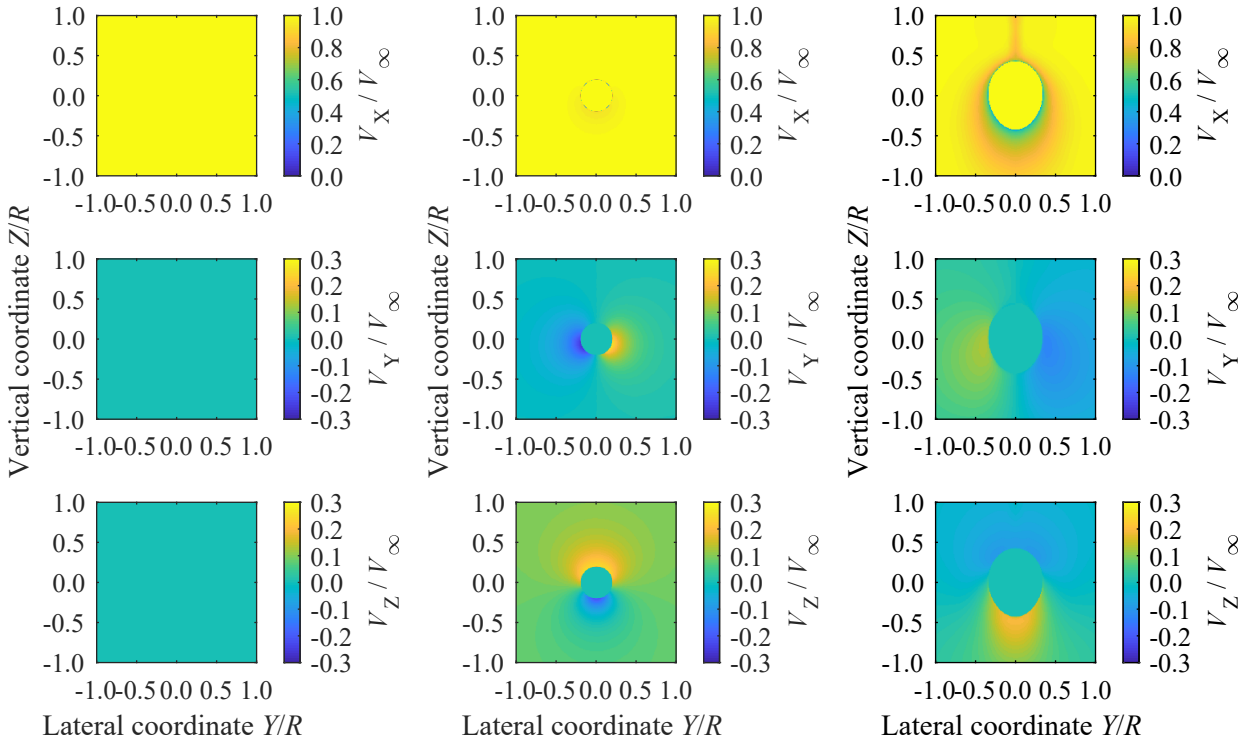

(a) Case 1: uniform inflow ($\alpha = 0$ deg)

(b) Case 2: nonzero angle of attack ($\alpha = 5$ deg)

(c) Case 3: boundary-layer ingestion

Figure 2 – Inflow fields considered in this study.

3.1.2 Isolated Performance

The isolated propeller performance was computed using the blade-element-momentum method described in Ref. [9]. This is a classical implementation of the blade-element momentum method with a simple sweep correction to have a first-order sensitivity to the modified performance when applying blade sweep. In the present work all analyzed blade planforms were unswept.
The computation of the installed performance requires a performance map of the isolated propeller over a range of rotational speeds (evaluated at constant freestream velocity) and a range of freestream velocities (evaluated at constant rotational speed). Examples are provided in Ref. [8]. For the optimizations including installation effects, such propeller performance map had to be obtained inside the optimization loop, for each considered propeller design.

3.1.3 Installed Performance

The installed performance is obtained by combining the inflow field with the isolated propeller performance map. The complete procedure is described in Ref. [8]. The inflow velocity field is recast into polar coordinates, after which effective changes in advance ratio are defined for each circumferential position of each radial blade segment due to the local changes in axial and circumferential velocity

components throughout the rotation. These changes in effective advance ratio are then used to predict the local change in performance due to the nonuniform inflow field. This is done based on the derivatives of the propeller performance maps computed for the isolated propeller with respect to the local effective advance ratio. The resulting quasi-steady blade loading is then transformed into the frequency domain and corrected for unsteady effects using the Sears function. The results are then transformed back into the time domain to obtain the final time-dependent blade loading throughout the rotation. The time-averaged performance is obtained by averaging over the circumferential coordinate, and is expressed in terms of installed thrust, torque, normal force, and side force on the propeller.

3.2 Propeller Acoustics

The acoustic emissions are computed using the frequency-domain method by Hanson [10], accounting for tonal-noise sources due to blade volume, steady blade loading, and unsteady blade loading. Broadband noise and tonal noise due to quadrupole sources are ignored. The acoustic analysis was focused on the propeller only; acoustic interference with surrounding airframe components and atmospheric propagation effects were not modeled.

4. Results

The analysis of the results is split into three parts. First, the optimization results for the isolated configuration in uniform inflow (Case 1) are discussed. Then, aerodynamic and acoustic optimizations for the installed configuration with 5-deg angle of attack (Case 2) are presented. Finally, the boundary-layer-ingestion configuration (case 3) is considered.

4.1 Isolated Propeller Optimization: Uniform Inflow (Case 1)

Optimizations were performed for the isolated propeller as a baseline for comparison with the results obtained from the optimizations including installation effects.

4.1.1 Aerodynamic Optimization

The aerodynamic optimizations were performed with the objective function defined by Eq. 2 and constraints defined by Eqs. 3 and 4. The objective was thus to minimize total energy consumption (based on propeller shaft power) over the climb and cruise phases of the reference mission. Figure 3 compares the optimized performance in terms of energy consumption over the reference mission and propeller efficiency for the different blade counts considered. The energy-consumption data are normalized with the results obtained with a blade count of $N_B = 3$ to highlight the relative impact of blade count on propeller performance. Figure 4 plots the corresponding optimized solidity, advance ratios in climb and cruise, and pitch settings in climb and cruise. Figure 5 plots top views of the untwisted planforms for the different cases considered.

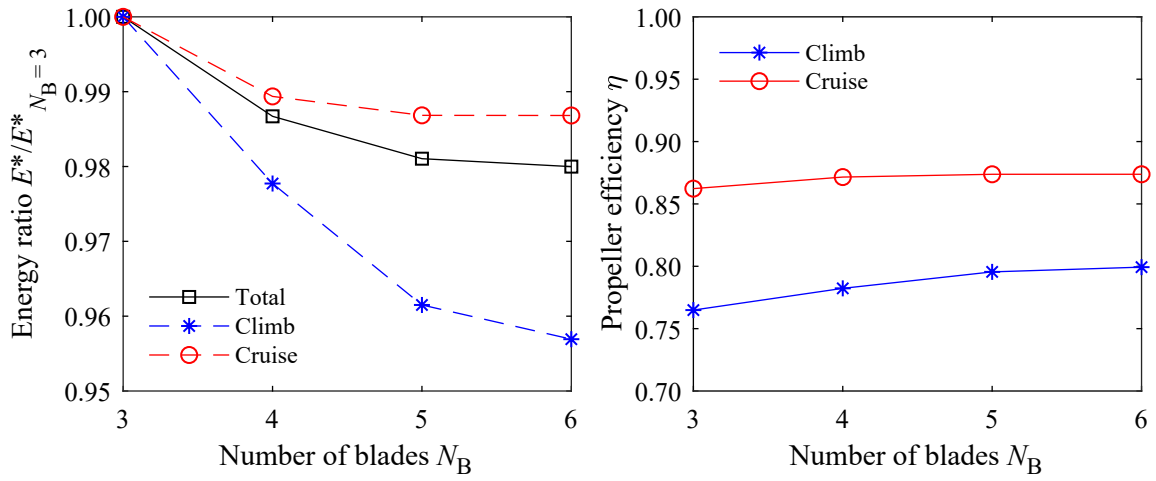

Figure 3 – Performance results for aerodynamic optimization in symmetric inflow. Energy normalized with optimal result obtained with 3 blades.

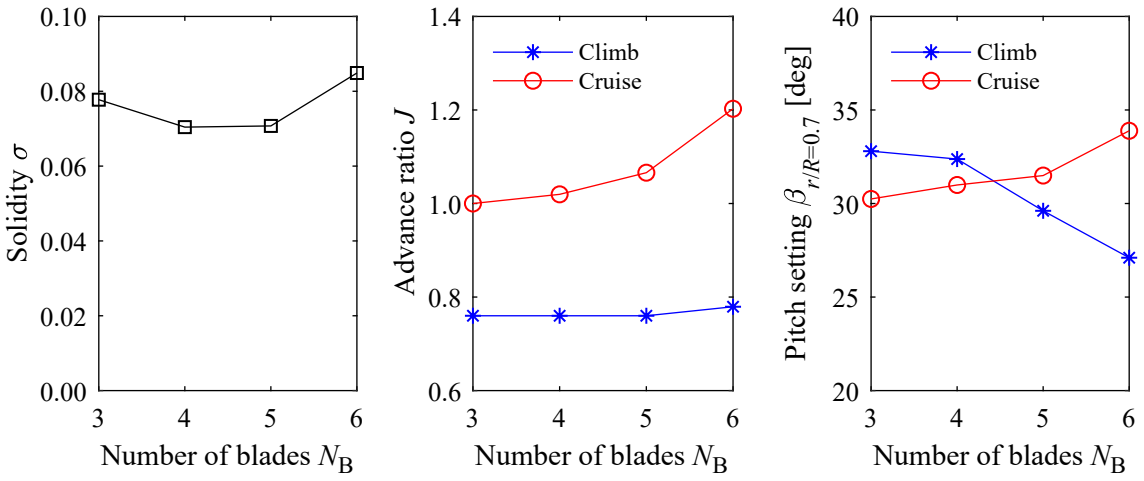

Figure 4 – Optimized solidity, advance ratios, and pitch settings for aerodynamic optimization in symmetric inflow.

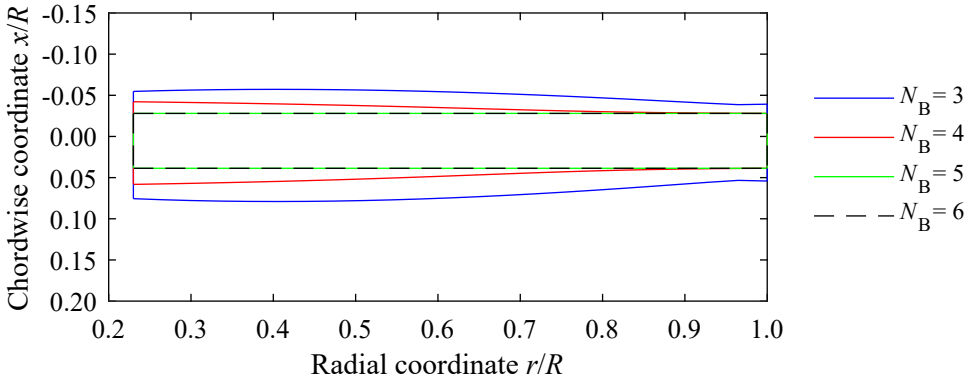

Figure 5 – Top view of untwisted planforms for aerodynamic optimization in symmetric inflow.

Figure 3 shows that the overall mission energy consumption (based on shaft power for given thrust requirement) was decreased by up to 2% by increasing the number of blades from 3 to 6. This reduction in energy consumption is the direct result of an increase in propeller efficiency. Although the overall disk loading was the same for all cases (due to the fixed thrust constraints and diameter), the blade loading was different due to the differences in solidity, advance ratio, and pitch setting (Fig. 4). The performance improvements obtained by increasing blade count were larger in the climb condition than in the cruise condition, because the blade loading is highest in the climb condition, and thus the blade count has the highest impact on the performance in that condition. For all cases, losses in the climb phase were minimized by minimizing the advance ratio. This maximizes the effective dynamic pressure at the blade sections, thereby enabling minimum lift coefficient of those blade sections for a given thrust. For the higher blade counts, the advance ratio was increased in the cruise phase in order to satisfy the thrust requirement. The pitch angle follows from a combination of thrust requirement and solidity, which define the total loading and sectional loading per blade.

The increase in performance with increasing blade count was mostly due to a reduction in induced losses. By increasing the number of blades, the absolute loading per blade decreases for a given disk loading. This is confirmed by Fig. 6, which displays the radial distributions of sectional lift loading. The applied scaling accounts for the differences in chord length and effective dynamic pressure between the designs. Combined with the increase in aspect ratio with increasing number of blades (Fig. 5), the reduction in lift loading leads to a reduction of induced losses. This is shown in Fig. 7, which displays the induced efficiency of the blade sections, defined as:

$$\eta_i = \frac{1 - \frac{v_t}{\Omega r}}{1 + \frac{v_a}{V_\infty}}, \tag{9}$$

with r the local radial coordinate, v_a and v_t the propeller-induced velocities in the axial and tangential directions, respectively, V_∞ the freestream velocity, and Ω the angular frequency of the propeller.

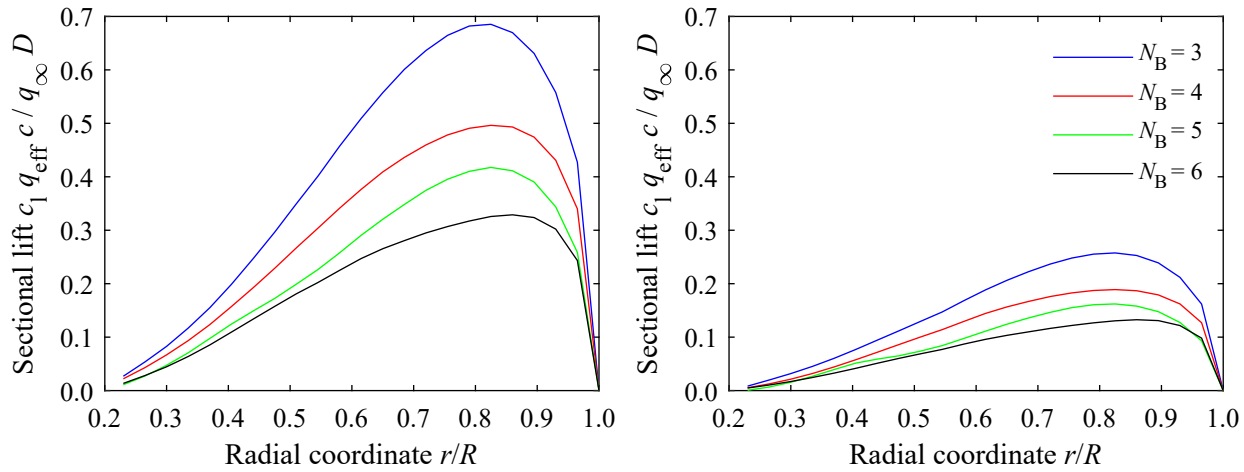

a) Climb **b) Cruise**

Figure 6 – Radial distributions of scaled sectional lift loading for aerodynamic optimization in symmetric inflow.

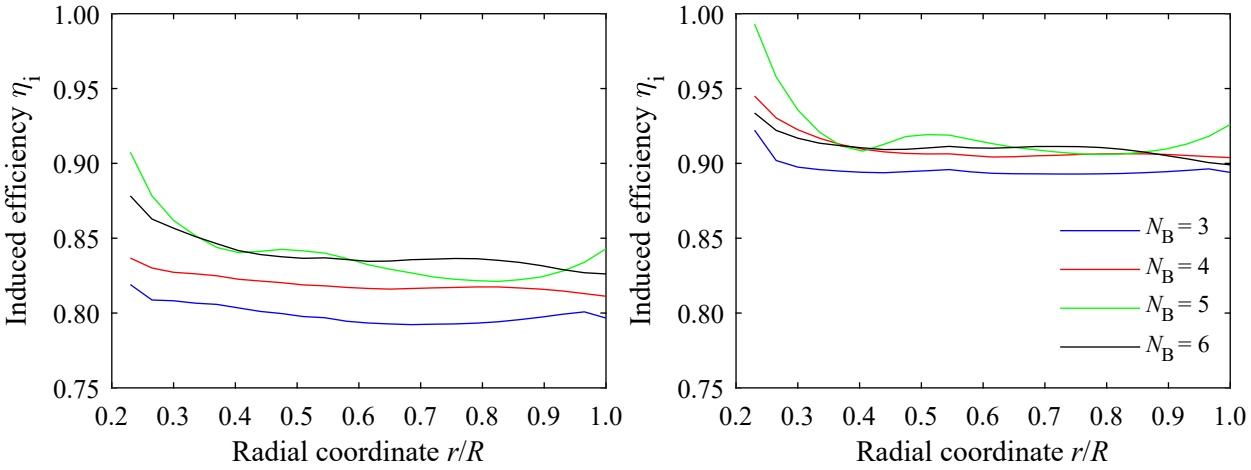

a) Climb **b) Cruise**

Figure 7 – Radial distributions of induced efficiency for aerodynamic optimization in symmetric inflow.

The induced efficiency accounts for induction losses due to swirl and axial acceleration. For a minimum-induced-loss design, the radial distribution of induced losses should be flat, and it can be seen that the optimizer approximately followed this requirement to optimize propeller performance. The induced losses are higher in the climb condition than in the cruise condition due to the higher blade loading in the climb condition. The induced efficiency, however, does not account for profile losses due to airfoil drag. For this reason, a profile efficiency was defined as:

$$\eta_\mathrm{p} = \frac{1 - \frac{c_d}{c_l}\frac{V_\infty + v_a}{\Omega r - v_t}}{1 + \frac{c_d}{c_l}\frac{\Omega r - v_t}{V_\infty + v_a}}, \tag{10}$$

with c_d and c_l the local sectional drag and lift coefficients, respectively.
Figure 8 displays the radial distributions of profile efficiency for the different optimal designs. It can be seen that the profile efficiency was approximately constant for the different designs, irrespective of blade count. Furthermore, the profile losses were about 4-5 times (climb) and 2.5 times (cruise) smaller than the induced losses (Fig. 7), and thus were not the dominant loss mechanism.
The constant profile efficiency with increasing blade count is due to a compromise between two opposing mechanisms: profile efficiency increased with decreasing solidity while it decreased with decreasing blade chord length due to a reduction in local Reynolds number. The reduction in induced losses with increasing blade count changes the ratio between induced and profile losses. Consequently, better performance can be achieved at higher blade count with lower solidity (see Fig.

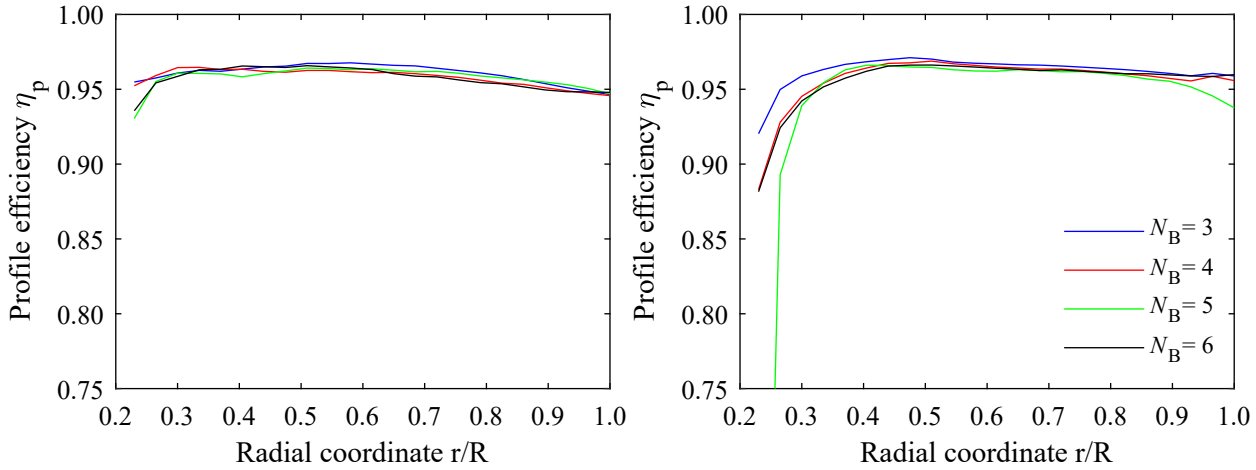

a) Climb **b) Cruise**

Figure 8 – Radial distributions of profile efficiency for aerodynamic optimization in symmetric inflow.

4, limited at $N_B = 5$ and $N_B = 6$ due to lower bound on chord), while at low blade count the solidity needs to be sufficiently high to limit the sectional lift coefficients and thereby the induced losses. A decrease in solidity enables an increase in local lift coefficient of the blade profiles for a given thrust requirement, which for the selected profiles led to an increase in profile efficiency. This means that the reference airfoils were designed for higher blade loading conditions than achieved at the thrust requirement considered in the present study. When also including airfoil optimization into the design loop, the performance increase with increasing blade count would reduce because at low blade count the blade profiles could be optimized to perform better at lower sectional lift coefficient. On the other hand, this increase in profile efficiency with increasing blade count was offset by a reduction in sectional Reynolds number, due to the reduction in sectional blade chord. As a result, the profile efficiency was approximately constant for all designs.

4.1.2 Acoustic Optimization

The acoustic optimizations were performed with the objective function defined by Eq. 6 and constraints defined by Eqs. 7 and 8. The objective was thus to minimize thrust-scaled noise emissions in the climb phase, accounting for the thrust requirements in both cruise and climb. The tradeoff between aerodynamic and acoustic performance was studied by imposing a variable inequality constraint on the energy consumption, which was specified as a fraction of increased energy consumption with respect to the aerodynamic optima discussed in the previous subsection.

Simulations were only performed for the cases with 3 and 4 blades, since the results for the cases with 5 and 6 blades were considered biased due to the active lower bound on the chord distribution. Figure 9 displays the change in thrust-scaled noise level compared to the baseline aerodynamic optimum with 3 blades, as a function of accepted energy penalty and blade count. The resulting impact on propeller efficiency is also included. The corresponding optimized values of the key design variables are displayed in Fig. 10, while Fig. 11 provides top views of the untwisted blade planforms. Figure 9 highlights the tradeoff between aerodynamic and acoustic propeller performance. For a given blade count, the optimized thrust-scaled noise levels decrease with increasing accepted energy penalty. This means that the accepted energy penalty is exploited to define a blade shape and operating conditions that result in lower propeller efficiency, but also lower noise levels at constant thrust requirement. Figure 10 shows that the significant reduction in noise levels with increasing accepted energy penalty is achieved by increasing the solidity, advance ratio, and collective pitch angle compared to the aerodynamic optimum. The increase in advance ratio at constant freestream velocity leads to a reduction in the helicoidal tip Mach number, as confirmed by Fig. 12. This is beneficial for the acoustic performance of the propeller [1], while disadvantageous for propeller efficiency. The increase in advance ratio is compensated for by an increase in solidity and pitch angle (Fig. 10) in order to still match the thrust requirements in climb and cruise. The increase in solidity can be recognized in the blade planform designs (Fig. 11) by the increase in chord length with increasing accepted energy penalty.

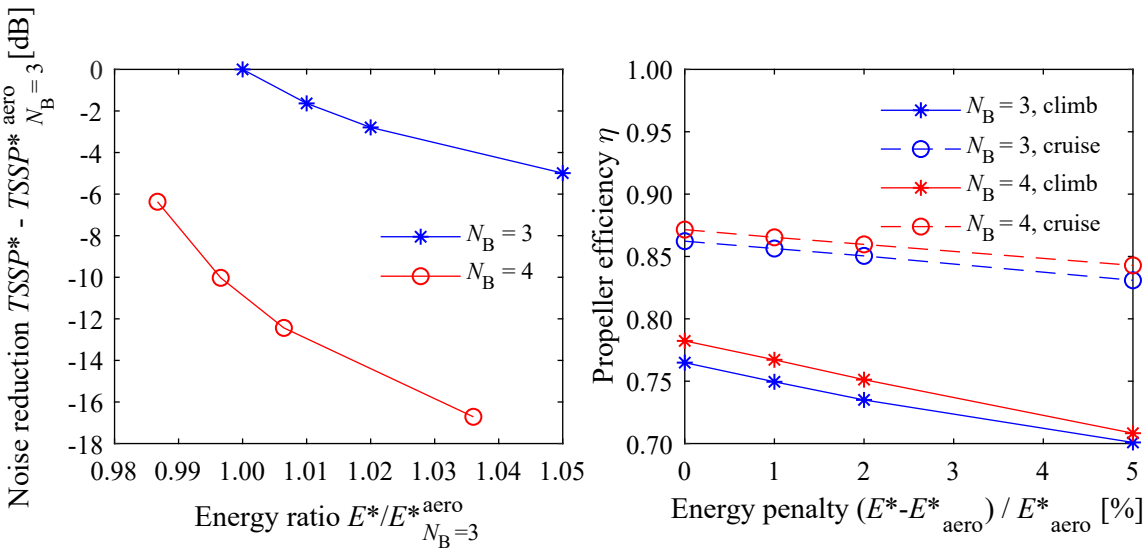

Figure 9 – Performance results for acoustic optimization in symmetric inflow.

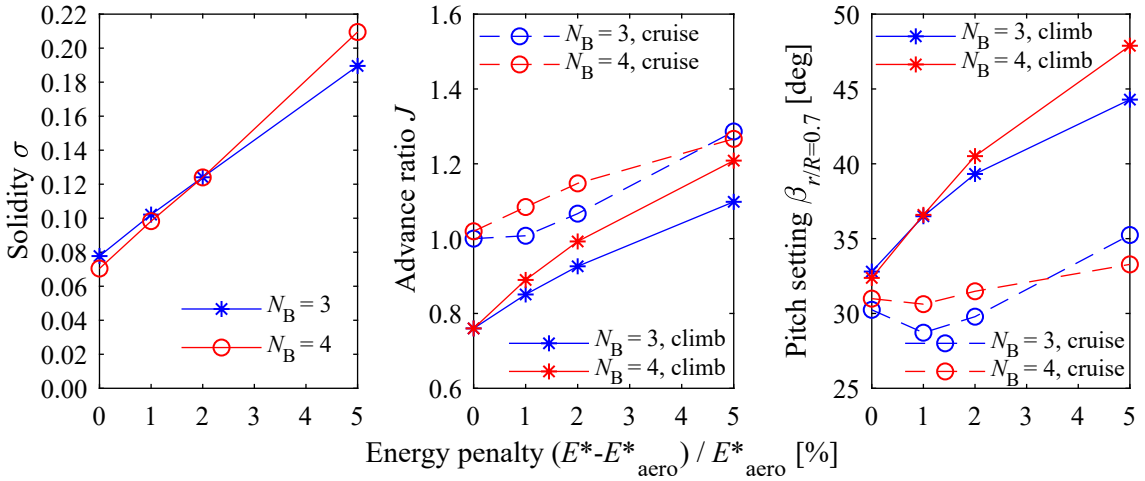

Figure 10 – Optimized solidity, advance ratios, and pitch settings for acoustic optimization in symmetric inflow.

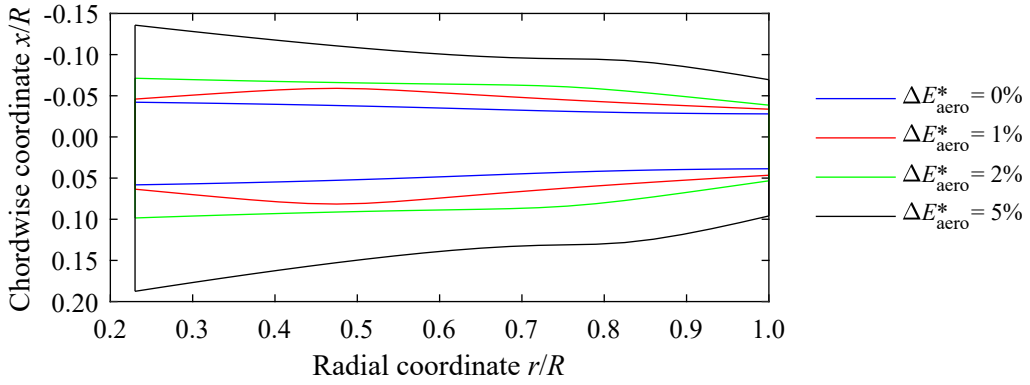

Figure 11 – Top view of untwisted planforms for acoustic optimization of the 4-bladed propeller in symmetric inflow.

Figure 13 shows how the increase in advance ratio to achieve increasing noise reduction requires an increase in relative blade loading, which penalizes induced efficiency. The acoustic optimization did not lead to a significant inboard shift of the loading distribution. The profile efficiency (not shown here) again was less affected, and even slightly increased in the climb condition because the original airfoil sections performed better at higher relative loading condition than achieved at the aerodynamic optimum. Earlier sensitivity studies such as the one presented in Ref. [6] have shown similar trends. It

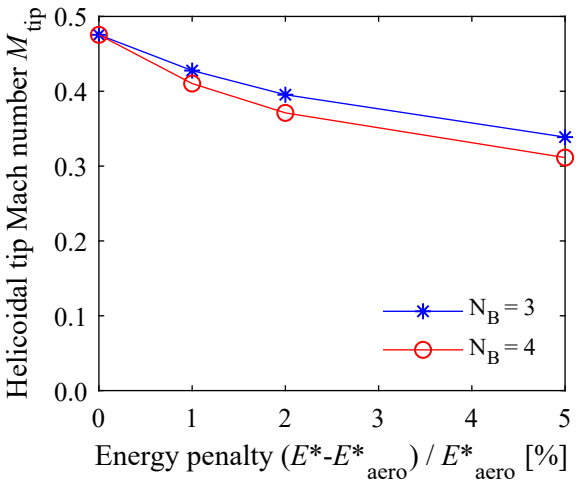

Figure 12 – Impact of allowed energy penalty on helicoidal tip Mach number for acoustic optimization in symmetric inflow.

should be noted that in the present study the sensitivity to the tip Mach number is especially high due to the low freestream Mach number of the reference aircraft considered. For applications operating at higher freestream Mach number, the acoustic benefit of reducing tip Mach number will be smaller because the baseline tip Mach number will be higher.

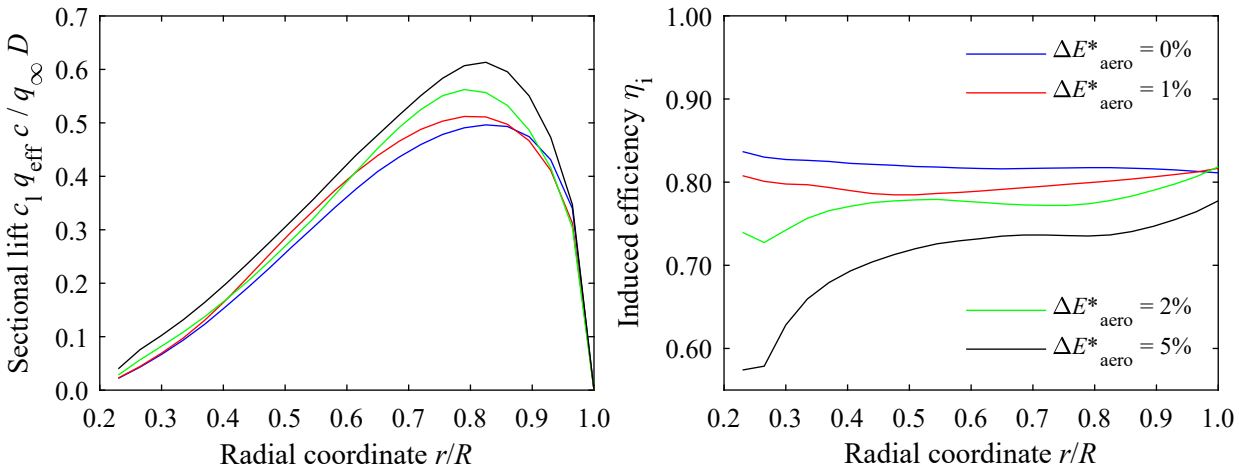

Figure 13 – Radial distributions of scaled sectional lift loading and induced efficiency versus allowed energy penalty for acoustic optimization of the 4-bladed propeller in climb in symmetric inflow.

The impact of blade count on the noise levels is two-fold. First, by increasing blade count from 3 to 4, the advance ratio can be further reduced while avoiding too high sectional blade loading. This allows a further reduction of tip Mach number (Fig. 12), thus lower noise. Furthermore, the increased blade count leads to increased acoustic interference between the pressure signals from the individual propeller blades [1]. An increase in blade count is thus beneficial for the noise levels both for aerodynamic and acoustic reasons. The increase in aerodynamic efficiency with increasing blade count is also observed for the acoustically optimized designs. For the considered design requirements, the 4-bladed propeller thus shows better performance than the 3-bladed design for both disciplines. Compared to the 3-bladed design, the 4-bladed propeller operates with about 6.5% lower energy consumption at equal noise level, or about 10 dB lower noise at equal energy consumption. For applications operating at higher freestream Mach number, the acoustic benefit of increasing the number of blades can be expected to be smaller than shown here, because the acoustic benefit of increasing advance ratio will be smaller.

4.2 Installed Propeller Optimization: 5-deg Angle of Attack (Case 2)

When operating in nonuniform inflow, the propeller performance and noise emissions change. Therefore, it was expected that accounting for this nonuniform inflow during the optimization process would enhance performance and reduce noise. This section presents the results for the propeller at 5-deg angle-of-attack (case 2, Fig. 2b).

The installed optimizations were performed with the same objective functions and constraints as for the isolated propeller. However, now the time-dependent loading was included in the aerodynamic and acoustic analysis. The resulting designs are referred to as 'installed designs'. The performance of the installed designs was compared to that obtained for the isolated propeller designs (optimized for performance in symmetric inflow). In this comparison, 3 different cases will be considered:

1. Isolated propeller design evaluated at 0-deg angle of attack;
2. Isolated propeller design evaluated at 5-deg angle of attack;
3. Installed propeller design evaluated at 5-deg angle of attack;

4.2.1 Aerodynamic Optimization

The aerodynamic optimizations were again performed with the objective function defined by Eq. 2 and constraints defined by Eqs. 3 and 4. In this case, the results were time-averaged over 1 rotation. Figure 14 compares the optimized performance in terms of propeller efficiency for the different blade counts. Figure 15 presents the corresponding values of the design variables. Figure 16 plots top views of the untwisted planforms for the cases with 3 and 4 blades. The results for 5 and 6 blades are omitted from this figure because all chord values were at the lower bound.

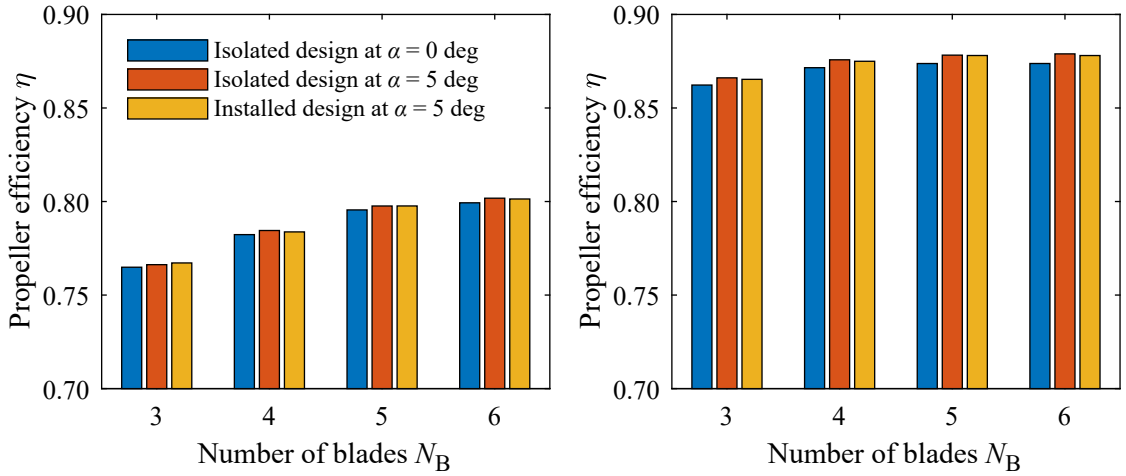

Figure 14 – Impact of 5-deg angle of attack on propeller efficiency in climb and cruise from aerodynamic optimization.

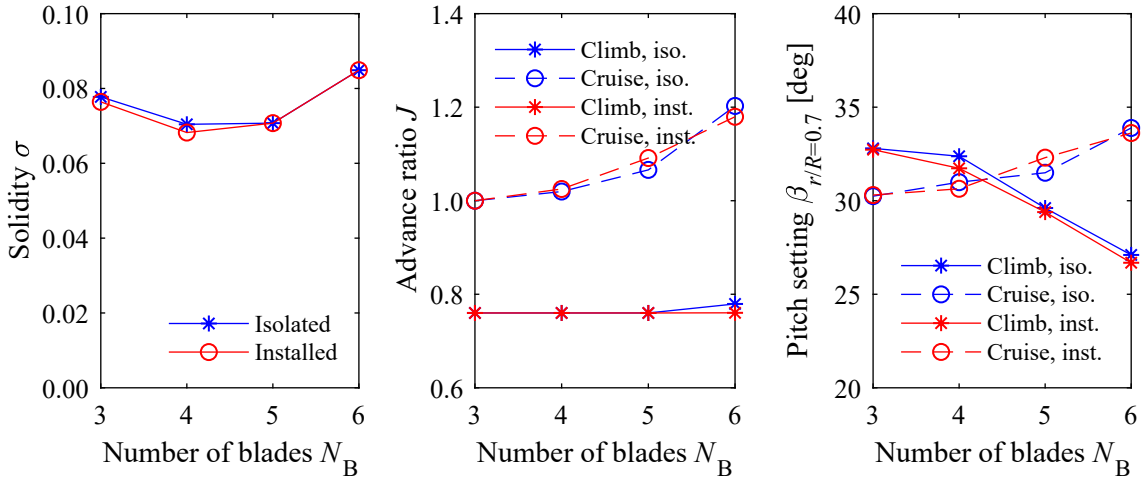

Figure 15 – Impact of 5-deg angle of attack on propeller design variables from aerodynamic optimization.

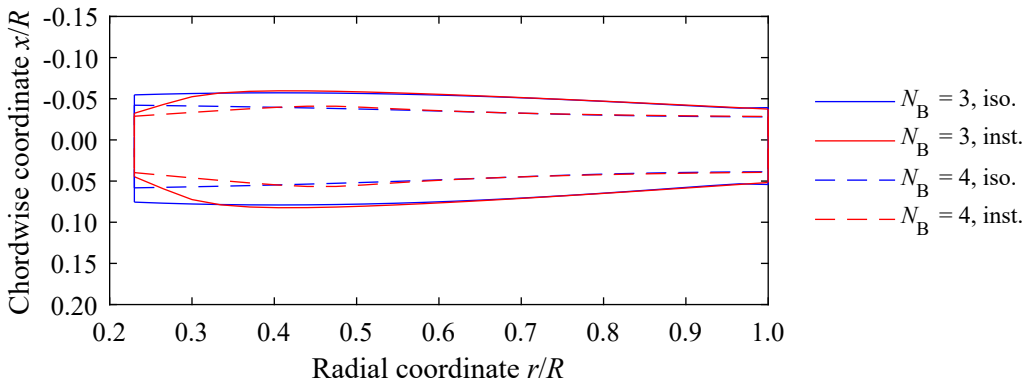

Figure 16 – Impact of 5-deg angle of attack on top view of untwisted planforms from aerodynamic optimization.

The operation at nonzero angle of attack modifies the thrust produced by the propeller. Consequently, the isolated propeller at 5-deg angle of attack produced higher than required thrust by about 0.5% for cruise and 1% for climb. For this reason, the comparison of aerodynamic performance of the different designs is not based on energy consumption, but on propeller efficiency instead. As expected, the impact of the 5-deg angle of attack on the propeller efficiency is small, and this is confirmed by Fig. 14. When taking the design obtained for symmetric inflow, and evaluating it at this nonuniform inflow condition, the propeller efficiency increased by 0.2-0.3% for all blade counts. This is due to the beneficial upwash experienced by the blade on the downgoing blade side. Note that the efficiency is defined here in the propeller reference system, hence thrust and torque are defined with respect to the propeller axis. When taking the forward force component in the flight direction, the remaining efficiency benefit would be negligible.

The 'installed design' is obtained by accounting for this installation effect inside the optimization loop. Considering the small impact of the 5-deg angle of attack on the propeller efficiency, this installed design performs about the same in terms of time-averaged propeller performance as the design obtained for symmetric inflow, with differences within $\pm 0.1\%$. This suggests that the difference between the performance of the isolated and installed designs is within the resolution of the analysis and optimization routine used. This is also reflected in the design variables and planform designs (Fig. 15, Fig. 16), which are similar between the two cases. For the cases with 3 and 4 blades, the blade solidity is 1-3% lower for the installed design than for the isolated design, while the cruise advance ratio is somewhat higher.

The blade planforms show that the reduction in solidity for the installed design is mostly due to a reduction in chord length on the inboard part of the blade, where the impact of the angle of attack on the local inflow to the blade sections is the largest due to the low tangential velocity associated with the rotation of the blade. A reduction in chord in this region would lead to an increase in relative loading, which is possible without induced-drag penalty due to the favorable upwash mechanism introduced by the operation at nonzero angle of attack. The advance ratio in climb remains at the lower bound to minimize swirl losses in that high-loading condition.

The difference in aerodynamic performance between the cases with and without flow nonuniformity considered in the design process naturally depends on the type of flow nonuniformity considered, and also on the objective function. By accounting for the unsteady effects inside the optimization, also time-dependent properties such as amplitude of unsteady blade loading could be minimized. This was not attempted in the present study.

4.2.2 Acoustic Optimization

The operation of the propeller in nonuniform inflow introduces unsteady blade loading, which represents an additional noise source. The acoustic optimization was performed for the installed case to quantify the opportunity to minimize this installation noise through dedicated planform design. As mentioned before, the isolated designs evaluated at nonzero angle of attack did no longer match the original thrust equality constraint. To still be able to assess noise levels versus combined energy

consumption over the climb and cruise parts of the mission, the energy ratios for the isolated designs were defined here by assuming that the propeller efficiency in installed conditions could also be achieved at the exact value of the thrust requirement. Therefore, a linear scaling based on thrust ratio was applied to the energy values of the isolated design evaluated in installed conditions. For this purpose, the climb and cruise phases of the mission were considered separately, and the energy consumption for these two flight phases was scaled with the ratio of required to installed thrust.
Figure 17 provides an overview of the change in thrust-scaled sound pressure level versus energy ratio obtained by including the installation effects in the design optimization. All results are evaluated at an angle of attack of 5 degrees, and are presented with respect to the aerodynamic optimum with 3 blades obtained without accounting for installation effects. The corresponding operational variables for the 4-bladed optima are provided in Fig. 18, while the planforms are plotted in Fig. 19. The results for the 3-bladed and 4-bladed cases were similar, and hence the 3-bladed cases are omitted from Figs. 18 and 19 for clarity of presentation.

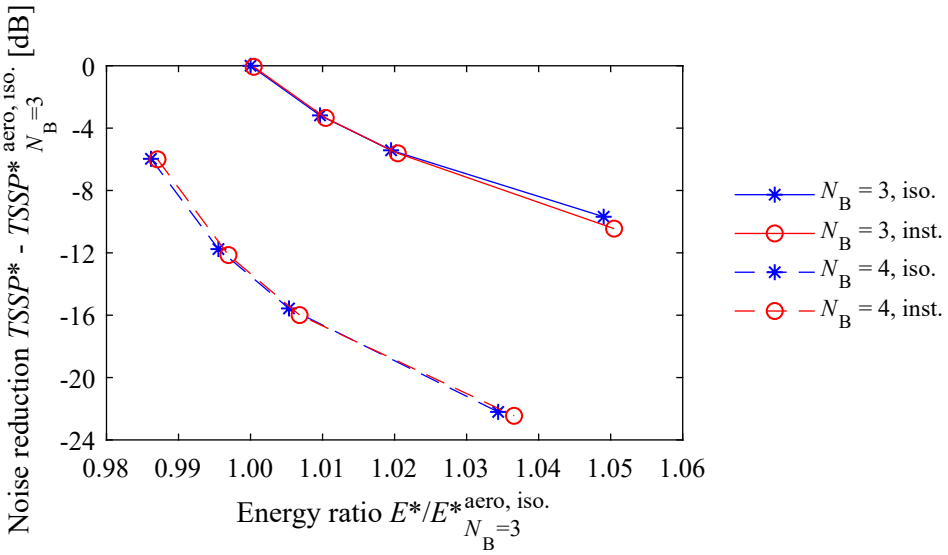

Figure 17 – Impact of 5-deg angle of attack on performance results from acoustic optimization.

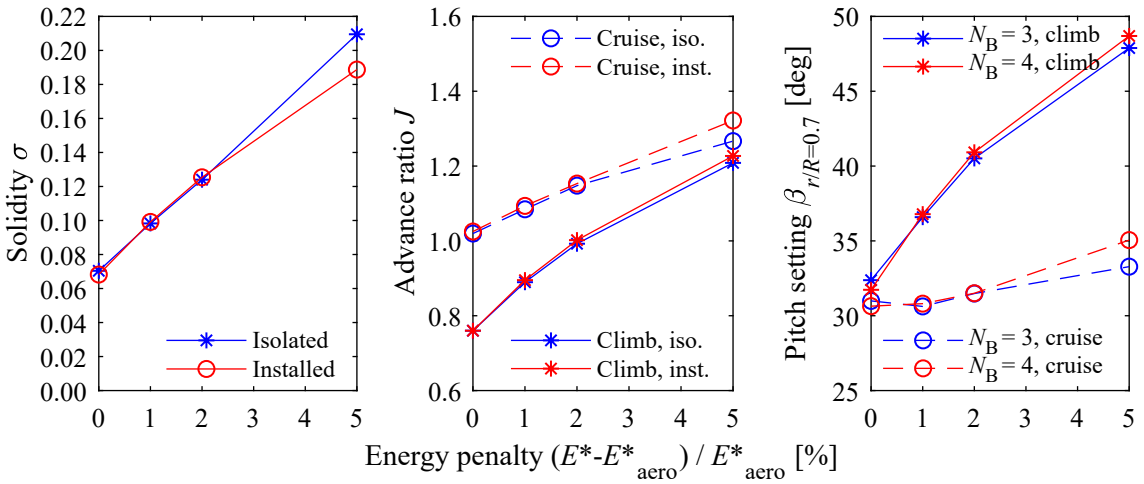

Figure 18 – Impact of 5-deg angle of attack on optimized solidity, advance ratios, and pitch settings from acoustic optimization of the 4-bladed propeller.

Figure 17 shows a negligible difference between the performance of the isolated and installed designs evaluated for the same 5-deg angle of attack case. Despite relatively large changes in planform design (Fig. 19), the performance of the isolated and installed designs is comparable. For the case with 3 blades, the installed design provides a minor noise reduction compared to the isolated design of around 0.5 dB at the maximum energy penalty considered. However, for the other energy

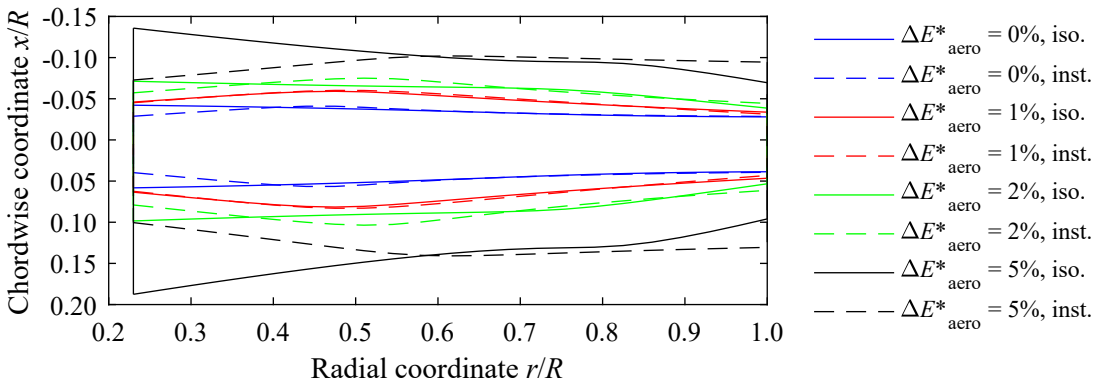

Figure 19 – Impact of 5-deg angle of attack on top view of untwisted planforms from acoustic optimization of the 4-bladed propeller.

penalties and all cases with 4 blades, the performance of the isolated and installed designs is within the resolution of the analysis and optimization chain. Similarly as for the aerodynamic optimization, compared to the isolated designs the solidity was decreased for the installed designs (only significant at the highest accepted energy penalty), while the advance ratio was increased. Figure 19 shows that the reduction in solidity again was due to a reduction in chord length on the inboard part of the blade, where the relative impact of the nonzero angle of attack on the inflow conditions is the largest. It is expected that the optimizer attempted to reduce the absolute loading in this region to reduce the noise due to unsteady blade loading. However, the overall impact on the noise levels is negligible because an increase in loading is required on the outboard part of the blade to still match the thrust constraint, which increases the noise associated with the steady loading. Overall, for the 5-deg angle-of-attack case, including installation effects inside the optimization did not lead to a significant aerodynamic or acoustic benefit compared to the isolated blade design.

4.3 Installed Propeller Optimization: Boundary-Layer-Ingestion (Case 3)

The nonuniform inflow representative of a boundary-layer-ingesting propeller at the rear fuselage (case 3, Fig. 2c) was only considered for aerodynamic optimization of the 3-bladed propeller. For this case, because the impact of the flow nonuniformity on the propeller thrust was much larger than for the angle-of-attack case (case 2), the operational conditions (advance ratios, pitch settings) of the isolated design were optimized in a separate step to achieve maximum performance in the nonuniform inflow field while adhering to the thrust requirements in climb and cruise. In this step, the planform design remained unchanged. The installed design was again obtained by including the installation effects into the full optimization procedure and thus resulted in different chord and twist distributions than for the isolated design, as well as different advance ratios and pitch settings.
Table 3 compares the change in aerodynamic performance obtained by including the installation effects into the planform design optimization, while Table 4 compares the resulting values of the design variables. Top views of the untwisted blade planforms are provided in Fig. 20, while Fig. 21 plots the radial distributions of chord and twist for both designs.

Table 3 – Impact of boundary-layer-ingestion inflow on performance from aerodynamic optimization of the 3-bladed propeller.

Parameter		Iso. design	Inst. design	(Inst.-Iso.)/Iso.
Energy	E_{total} [MJ]	59.7	59.4	-0.4%
	E_{climb} [MJ]	14.0	13.8	-1.5%
	E_{cruise} [MJ]	45.7	45.6	-0.1%
Prop. efficiency	η_{cl}	0.81	0.82	+1.5%
	η_{cr}	0.95	0.95	+0.0%

Table 4 – Impact of boundary-layer-ingestion inflow on propeller design variables from aerodynamic optimization of the 3-bladed propeller.

Parameter		Iso. design	Inst. design	(Inst.-Iso.)/Iso.
Advance ratio	J_{cl}	0.76	0.76	+0.0%
	J_{cr}	1.0	1.0	+0.0%
Collective pitch	β_{cl} [deg]	31.6	30.0	-5.0%
	β_{cr} [deg]	28.1	27.7	-1.6%
Solidity	σ	0.078	0.098	+26.0%

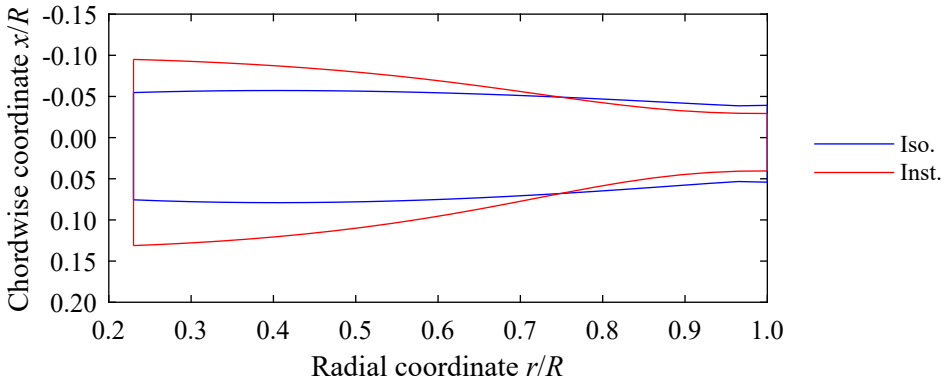

Figure 20 – Impact of boundary-layer-ingestion inflow on top view of untwisted planforms for aerodynamic optimization of the 3-bladed propeller.

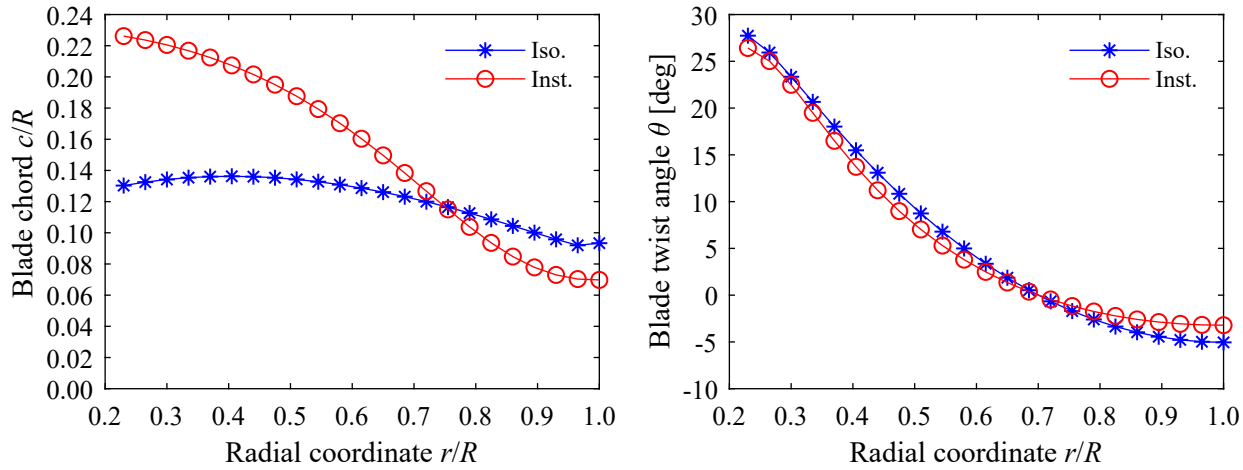

Figure 21 – Impact of boundary-layer-ingestion inflow on radial distributions of chord and twist for aerodynamic optimization of the 3-bladed propeller.

Table 3 shows that for this installation case, accounting for installation effects in the optimization resulted in a 0.4% reduction in energy consumption over the mission compared to the isolated design. This was mostly due to an increase in propeller efficiency of 1.5% in the climb phase. Note that the definition of propeller efficiency was based on freestream conditions, which partially explains the high values compared to installation cases 1 and 2.

From Table 4 it is concluded that the increase in efficiency of the installed design was obtained through an increase in blade solidity. This increase in solidity was focused on the inboard part of the blade as shown by the blade planforms (Fig. 20) and chord distributions (Fig. 21). In this region, the low axial velocity led to a reduction in effective advance ratio, which was exploited by the optimizer to improve performance. At the same time, the twist on the inboard part of the blade was decreased compared to the isolated design (Fig. 21) in order to limit the resulting angles of attack at the blade sections. Future work will assess the acoustic benefits of accounting for installation effects for a complicated nonuniform inflow field like the one considered here.

5. Conclusions

This paper has presented the results of aerodynamic and acoustic propeller optimizations for symmetric and nonuniform inflow conditions. Based on the results, the following conclusions are drawn:

- An increase in the blade count increases aerodynamic and acoustic propeller performance, both for isolated and installed conditions. Aerodynamic performance is improved due to reduced induced losses, while acoustic performance is improved due to the larger potential to reduce tip Mach number for a given induced loss.
- For a given blade count and the freestream Mach number considered in this paper, noise is most effectively reduced by decreasing the tip Mach number, through an increase in propeller advance ratio at given freestream conditions. This results in a reduction of induced efficiency. Therefore, the aerodynamic and acoustic performance of a propeller are conflicting objectives. The reduction in noise obtained for a given reduction in energy efficiency depends on the blade count, with higher potential for noise reduction at higher blade count.
- Accounting for installation effects in the aerodynamic design of a propeller for maximum time-averaged energy efficiency does not significantly change the performance and design for a simple nonuniform inflow case like a 5-deg angle of attack. For the more complex case of a boundary-layer-ingestion configuration performance benefits can be obtained, with a 0.4% reduction in energy consumption compared to the design for symmetric inflow conditions, and a maximum efficiency benefit of 1.5% in the climb phase.
- Accounting for installation effects in the acoustic design of a propeller for minimum noise emissions at a given energy-efficiency level only leads to minor noise reductions of at most 0.5 dB for a simple nonuniform inflow case like a 5-deg angle of attack. The blade planform design and operational variables were not significantly modified for this case compared to the design for symmetric inflow conditions.

Future work will assess the potential for improved aerodynamic and acoustic performance of installed propellers for more complex interaction cases, including an evaluation of the impact of blade sweep and airfoil design and the sensitivity of the results to the tip Mach number. Such results will help to decide whether installation effects need to be accounted for during the preliminary design stage to achieve low-noise, high-efficiency propellers for future sustainable aircraft.

Acknowledgments

The authors would like to thank Nando van Arnhem, Sparsh Garg, and Martijn van Sluis for providing the nonuniform inflow fields.

Contact Author Email Address

mailto: T.Sinnige@tudelft.nl

Copyright Statement

References

[1] Magliozzi B, Hanson D B and Amiet R K. Propeller and Propfan Noise, *Aeroacoustics of Flight Vehicles: Theory and Practice. Volume 1: Noise Sources*. ed: Hubbard H H. NASA Langley Research Center, 1991.

[2] Marinus, B. *Multidisciplinary Optimization of Aircraft Propeller Blades*. PhD thesis, École Centrale de Lyon. 2012.

[3] Pagano A, Federico L, Barbarino M, Guida F and Aversano, M. Multi-Objective Aeroacoustic Optimization of an Aircraft Propeller. *12th AIAA/ISSMO Multidisciplinary Analysis and Optimization Conference*, Victoria, BC, Canada, AIAA Paper 2008-6059, 2008.

[4] Gur O and Rosen A. Optimization of Propeller Based Propulsion System. *Journal of Aircraft*, Vol. 46, No. 1, pp. 95-106, 2009.

[5] Ingraham D, Gray J and Lopes L V. Gradient-Based Propeller Optimization with Acoustic Constraints. *AIAA Scitech 2019 Forum*, San Diego, CA, USA, AIAA Paper 2019-1219, 2019.

[6] Miller C J and Sullivan J P. Noise constraints effecting optimal propeller designs. *SAE General Aviation Aircraft Meeting and Exposition*, Wichita, KS, USA, SAE Paper 850871, 1985.

[7] Pagano A, Barbarino M, Casalino D and Federico L. Tonal and Broadband Noise Calculations for Aeroacoustic Optimization of a Pusher Propeller. *Journal of Aircraft*, Vol. 47, No. 3, pp. 835-848, 2010.

[8] van Arnhem N, de Vries R, Sinnige T, Vos R, Eitelberg G and Veldhuis L L M. Engineering Method to Estimate the Blade Loading of Propellers in Nonuniform Flow. *AIAA Journal*, Vol. 58, No. 12, pp. 5332-5346, 2020.

[9] Geng X, Hu T, Liu P, Sinnige T and Eitelberg G. Analysis of Thrust-Scaled Acoustic Emissions of Aircraft Propellers and Their Dependence on Propulsive Efficiency. *32nd Congress of the International Council of the Aeronautical Sciences*, Shanghai, China, ICAS Paper 2020-0751, 2021.

[10] Hanson D B. Noise of Counter-rotation Propellers. *Journal of Aircraft*, Vol. 22, No. 7, pp. 609-617, 1985.